This document was prepared for the ETI by third parties under contract to the ETI. The ETI is making these documents and data available to the public to inform the debate on low carbon energy innovation and deployment.

Programme Area: Marine

Project: PerAWAT

Title: Development of Free Surface Wave Model for an Axial Flow Tidal Turbine

Abstract:

The objective of this deliverable is to extend the existing computational model of a full scale tidal turbine to account for the effect of regular free surface waves. The new model is presented in this report, and its wave modelling capability is demonstrated.

Context:

The Performance Assessment of Wave and Tidal Array Systems (PerAWaT) project, launched in October 2009 with £8m of ETI investment. The project delivered validated, commercial software tools capable of significantly reducing the levels of uncertainty associated with predicting the energy yield of major wave and tidal stream energy arrays. It also produced information that will help reduce commercial risk of future large scale wave and tidal array developments.

Energy Technologies Institute

PerAWaT

WG3 WP1 D5: Development of Free Surface Wave Model for an Axial Flow Tidal Turbine

Authors C. F. Fleming, S. C. McIntosh, R. H. J. Willden

Version 0.1

Date 1/3/13

Revision History		
Issue / Version	**Issue Date**	**Summary**
0.1	15/3/13	First draft for review by GH

Executive Summary

The objective of this deliverable is to extend the existing computational model of a full scale tidal turbine to account for the effect of regular free surface waves. The new model is presented in this report, and its wave modelling capability is demonstrated.

The starting point for this model is that which has been presented in WG3 WP1 D4. In that work, an 18 m diameter rotor is simulated in a variety of sheared and blocked flows. A body-fitted grid is used to capture the rotor geometry. Rotor motion is achieved by defining a sliding mesh interface between the rotor mesh and the surrounding stationary channel mesh. For this model, and preceding models at experimental scale, the effects of the free surface were found to be insignificant, and hence the rigid lid approximation was used.

In this work, the volume-of-fluid (VOF) model is used for free surface tracking. A periodic velocity boundary condition is applied upstream of the turbine which propagates waves downstream, in addition to the mean current. A wave damping zone is defined downstream of the device to prevent reflection of waves back upstream. Model accuracy is quantified through the changes in wave height and length as waves propagate from the inlet to the outlet of the computational domain.

The turbine is simulated in operation in this wave field to predict power, thrust and wake development. The effect of the wave field on the turbine is identified through frequency analysis.

The model is shown to adequately reproduce an open channel flow with free-surface waves, and can be used to study the effect of this class of flows on tidal turbine operation. Wave parameters such as amplitude, wavelength and direction may be altered, enabling future parametric studies in WG3 WP1 D5 and D6.

Table of Contents

1 Introduction

This report describes the extension of an existing computational model of a tidal turbine to include the effects of free surface waves. The existing model has been developed in previous work by the authors in WG3 WP1 D1−4. It has been used to investigate the effects of yawed and sheared flows on tidal turbine performance. The effects of vertical position and lateral spacing of turbines has also been examined. A future objective of the PerAWaT project is to determine the influence of free surface waves on the performance of tidal turbines. This deliverable introduces the free surface modelling technique used, and a demonstrative simulation is presented.

The model geometry and boundary conditions are described in section 2. Wave motion is imparted through the specification of an unsteady velocity profile upstream of the turbine. Waves are damped downstream of the turbine to prevent reflection back upstream. Periodic lateral boundary conditions are used to enable waves to travel in directions other than that of the mean flow. The theory behind these boundary conditions is presented in sections 2.2.1−2.2.3. Rotor motion, turbulence modelling and spatial discretisation are also discussed in section 2.

Appropriate wave parameters (height and length) are discussed in section 3. The numerical beach downstream of the turbine must be tuned to damp the oncoming waves. The appropriate damping coefficient is found through a systematic study presented in this section.

The results of a demonstrative simulation are presented in section 0. Comparisons of thrust, power and wake velocity are made with the rigid lid model from WG4 WP1 D4. The effects of the wave field on the turbine are highlighted through frequency analysis of the blade forces.

2 Description of model

2.1 Geometry

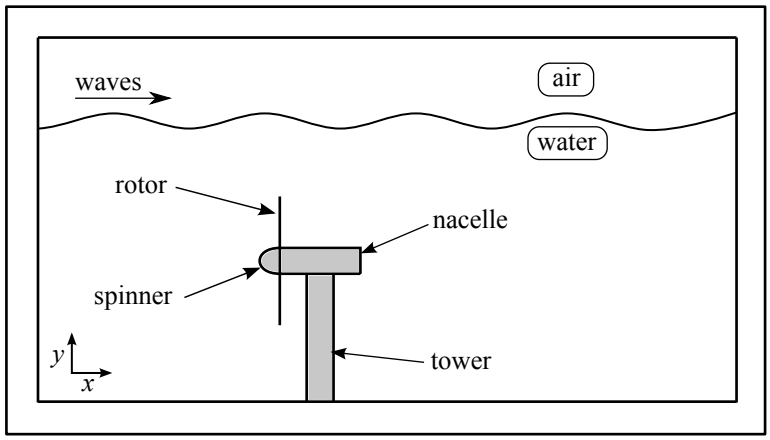

Figure 1: Schematic diagram of computational model with the significant features labeled.

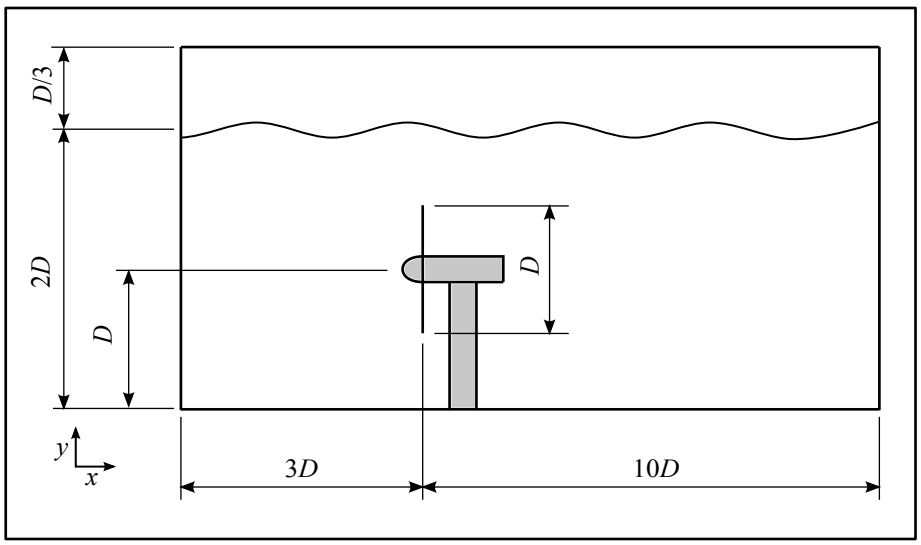

Figure 2: General dimensions of the computational model. The rotor diameter, D, is 18 m.

A three-bladed axial flow turbine is simulated in a channel of rectangular cross section. The rotor geometry has been provided by the PerAWaT consortium. The rotor measures 18 m in diameter. The nacelle is modelled as a simple cylinder, following Gretton & Ingram (2011). It measures 3 m in diameter, 10.1 m in length, and the spinner is an ellipsoid with a 1:1.5 axis ratio. The tower is represented by a straight cylinder of 2 m diameter.

2.2 Computational Setup

2.2.1 Wave Modelling

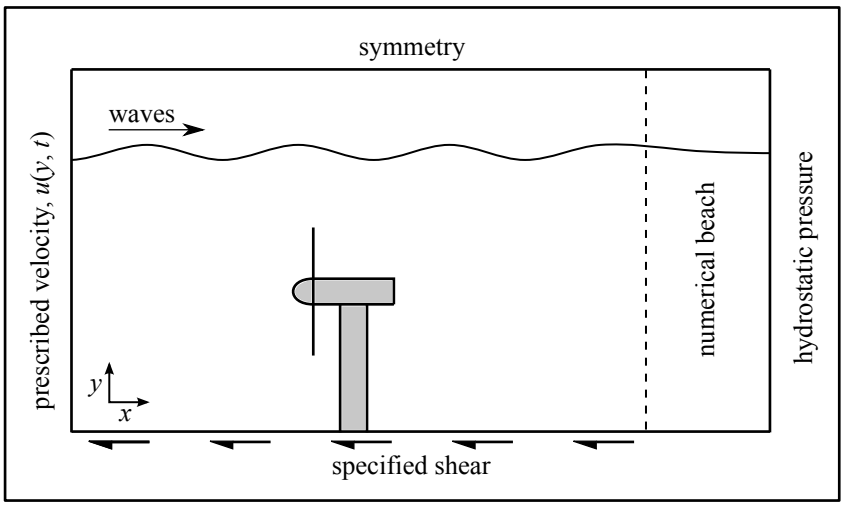

Figure 3: Schematic diagram of the computational model showing the boundary conditions applied. A periodic boundary condition is applied at vertical planes on either side of the turbine.

A two-phase volume-of-fluid (VOF) model is used to simulate wave motion at the free-surface. In the VOF model, a transport equation for volume fraction α is solved alongside the RANS equations. The volume fraction indicates the amount of water and air in a given mesh element, with $\alpha = 0$ corresponding to water and $\alpha = 1$ corresponding to air.

The mean water level is set at $2D$ (36 m). The region of air above the free surface is D / 3 (6 m) high. A symmetry condition is applied at the upper boundary of the air region.

Wave orbitals are set in motion by specifying an unsteady velocity boundary condition at the domain inlet, which is located $3D$ (54 m) upstream of the rotor plane. One of the objectives of later work will be to investigate the effect of free surface waves travelling at a relative angle to the streamwise direction. Therefore the wave model must allow for waves to propagate in the streamwise (x) and transverse (y) directions.

Wave motion is achieved by superimposing a wave-induced velocity profile onto a mean velocity profile. The unsteady velocity profile is defined using first order linear (Airy) wave theory,

$$u_x = U_x + \frac{gkH}{2\omega}\frac{\cosh[k(d+y_d)]}{\cosh kd}\cos\phi_w \cos\alpha \tag{1}$$

$$u_x = U_x + \frac{gkH}{2\omega}\frac{\cosh[k(d+y_d)]}{\cosh kd}\cos\phi_w \cos\alpha \tag{2}$$

$$u_y = \frac{gkH}{2\omega}\frac{\sinh[k(d+y_d)]}{\cosh kd}\sin\alpha \tag{3}$$

where x, z, and y, are the streamwise, transverse and vertical directions respectively, u is velocity, U is the velocity of the mean flow, g is acceleration due to gravity, H is wave height, k is the wave number, defined by $k = 2\pi / \lambda$, y_d is the vertical distance from the free surface, and ϕ_w is the wave yaw angle. The phase angle α is defined as

$$\alpha = xk_x + xk_z - \sigma t \tag{4}$$

where the directional wave numbers are defined as $k_x = k\cos\phi_w$ and $k_z = k\sin\phi_w$, and t is time. σ is the wave frequency with respect to the turbine

$$\sigma = \omega + k_x U_x + k_z U_z \tag{5}$$

where ω is the wave frequency with respect to the mean flow,

$$\omega = \sqrt{kg\tanh kd}\,. \tag{6}$$

A wave height of 1 m and wavelengh of 30 m are chosen for the demonstration case presented in section 0.

2.2.2 Downstream boundary condition

A constant free-surface height is desirable at the outlet of the domain, as it allows a steady hydrostatic pressure gradient to be applied, aiding solution stability. However, if the water height is constrained at the outlet, free surface waves will reflect back upstream upon reaching the outlet. In order to avoid this, a damping zone is defined for one full wavelength upstream of the outlet. Wave motion is damped through the addition of a sink term, S, to the momentum equation for the mesh elements in this region,

$$S = -C\left(\frac{1}{2}\rho\,|v|v\right)\left(1 - \frac{y - y_{\mathrm{fs}}}{y_{\mathrm{b}} - y_{\mathrm{fs}}}\right)\left(\frac{x - x_{\mathrm{s}}}{x_{\mathrm{e}} - x_{\mathrm{s}}}\right)^2 \tag{7}$$

where C is a damping coefficient, ρ is fluid (water or air) density, v is velocity in the vertical (y) direction, and x and y are streamwise and vertical coordinates respectively. The subscripts 'b' and 'fs' refer to the bottom of the channel and the free-surface, while the subscripts 's' and 'e' refer to the start and end of the damping region. An appropriate value for the damping coefficient C has been determined following a parametric study, which is described in section X. The domain outlet is located 10D (180 m) downstream of the rotor plane.

2.2.3 Lateral boundary condition

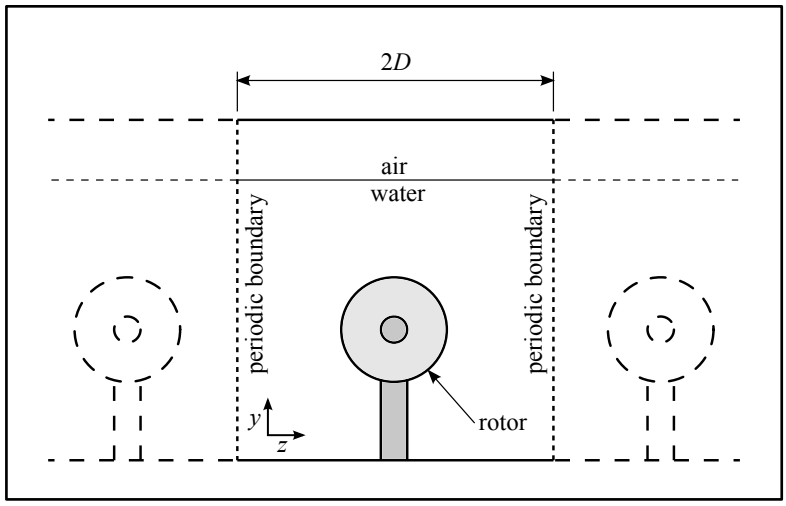

Figure 4: Front view of the turbine, showing periodic boundary conditions at the sides of the computational domain.

Periodic boundary conditions are applied at the sides of the computational domain, simulating an infinite fence of turbines. The spacing of turbines is equivalent to the domain width, with is 2*D* (36 m). The periodic boundaries also allow free surface waves to travel at an angle relative to the streamwise direction.

2.2.4 Rotor Motion

Angular motion of the rotor is achieved via the sliding mesh technique available in ANSYS FLUENT. The computational domain is divided into two regions: an inner cylindrical region which encloses the rotor, and an outer region which encompasses the far field elements of the model. Both regions are discretised with three-dimensional mesh elements. The inner mesh region is allowed to rotate relative to the outer region, simulating rotor motion. The rotor advances 0.8° every timestep. Temporal convergence is demonstrated in the torque history plots presented in the Appendix.

2.2.5 Turbulence Modelling

The *k-ω* SST model is used for turbulence closure, following previous work by the authors (McIntosh, Fleming, & Willden, 2010) and for consistency with the full scale turbine model in WG3 WP1 D4 (Fleming, McIntosh, & Willden, 2012).

2.2.6 Spatial Discretisation

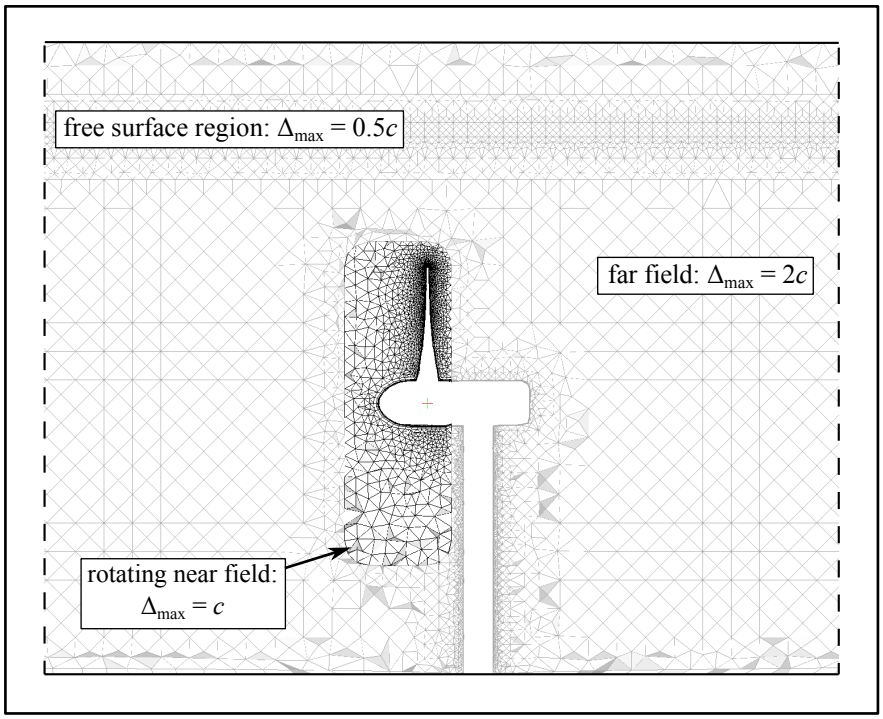

Figure 5: Vertical midplane slice through the computational model, showing maximum element size, Δ_{max}, at various locations in terms of the blade chord length at 80% rotor radius, $c = 1$ m.

As mentioned in section 2.2.4, the computational domain is made up of an inner cylindrical region containing the rotor, and an outer region which encompasses the stationary elements of the model (nacelle, tower, and domain boundaries). Both regions are filled with tetrahedral mesh elements. Maximum element sizes are given in Figure 5, relative to the chord length of the rotor blade at 80% rotor radius, $c = 1$ m.

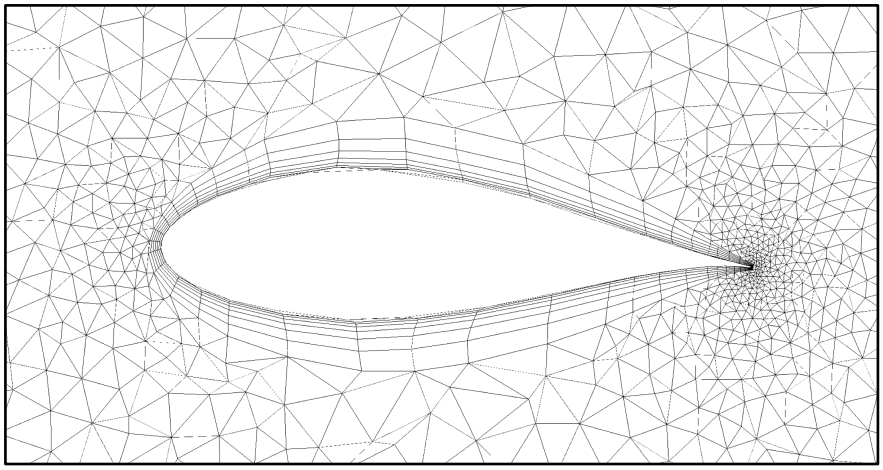

Figure 6: Cutplane through the rotor blade mesh at 80% radius, where the chord length $c = 1$ m.

The near field mesh which encloses the rotor is taken from previous work by the authors, details of which are given in WG3 WP4 D4 (Fleming, McIntosh, & Willden, 2012).

The far field mesh is generated using the Octree algorithm detailed in WG3 WP1 D3 (McIntosh, Fleming, & Willden, 2011). The maximum element size in the far field is $2c$, and a lower limit of $0.5c$ is prescribed in the vicinity of the free surface. This level of free-surface discretisation is shown to be adequate by Figure 9 and Figure 10 in section 0.

3 Development of Wave Model

As mentioned in section 2.2.2, tuning of the numerical beach is required to limit both wave reflections and outlet free-surface fluctuations. Tuning is accomplished via a systematic study into the effects of the beach damping coefficient C on wave reflection and propagation in the vicinity of the numerical beach.

An empty 106 m long channel with the same cross section and mesh resolution as that discussed in section 2.2 is constructed. Three waves of wave number $k = 0.209$ and significant height $H = 1$ m are introduced at the inlet boundary and convected downstream. The influence of the beach damping coefficient is assessed via a number of simulations where the damping level is varied from $C = 32$ to $C = 12800$. The resulting free surface evolution of three such cases is illustrated in Figure 7.

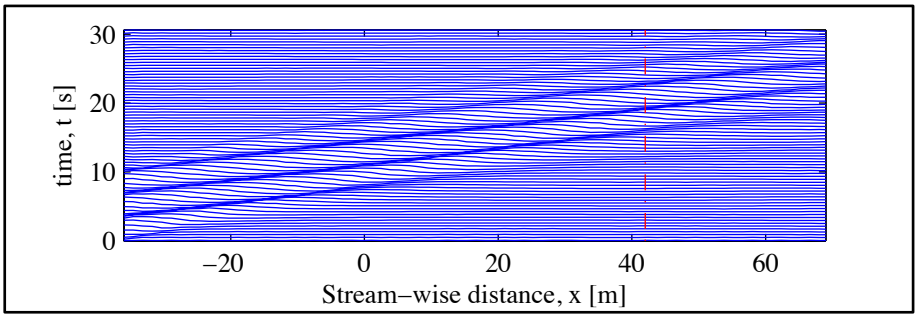

(a) C= 32

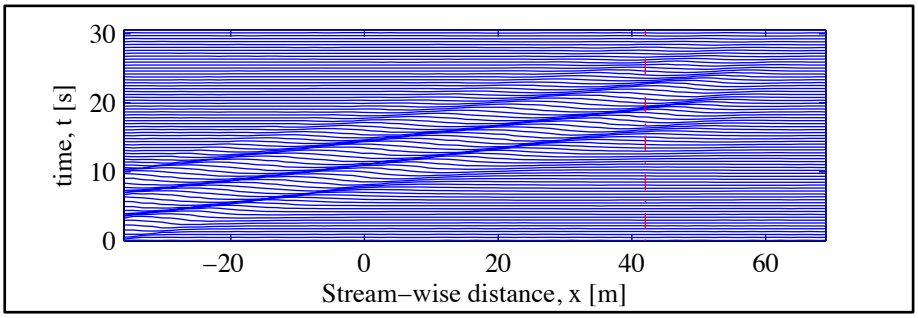

(b) C= 1280

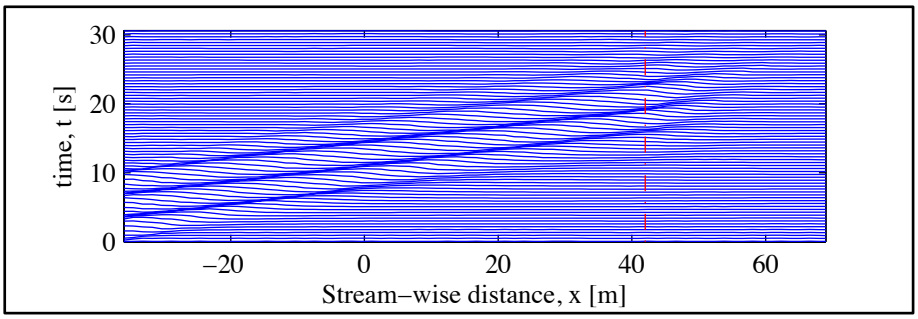

(c) C= 12800

Figure 7: Impact of beach damping on the absorption / reflection of a packet of three waves (λ=30m, H=1m).

For each plot, an initially flat free surface is perturbed by a set of three waves convecting from left to right. After approximately 10 seconds the inlet boundary condition returns to a level surface uniform velocity constraint.

Convection of the waves through the domain is clearly visible in Figure 7. Three dark diagonal lines locate each wave crest as a function of both position and time; with the inverse gradient of each corresponding to the wave speed.

Whilst wave reflections (right to left running diagonal lines) appear absent in all three cases, Figure 7, the level of damping is shown to strongly influence wave transmission through the beach zone. The set of three waves pass unhindered through the beach zone for the lowest damping case (C = 32), Figure 7 (a). An oscillation of the outlet free surface results, negatively impacting solution stability. Increasing the beach damping coefficient (C = 1280) results in far greater wave dissipation limiting free surface oscillations at the channel outlet, Figure 7 (b). A further increase the beach damping coefficient (C = 12800) leads to a shorter length over which the waves are effectively dissipated, Figure 7 (c).

A damping coefficient of C = 10000 is selected from this study, effectively damping oncoming waves within a distance of one wavelength whilst limiting reflections back into the numerical domain.

4 Demonstration of Wave Model

Functionality of the blade resolved tidal turbine model including free surface waves is now demonstrated. The turbine model described in section 2.2 is run at a tip-speed-ratio of $\lambda = 4.5$ with a uniform current of 2 m s^{-1} and free surface waves ($H = 1$ m, $k = 0.209$). To allow for complete wake propagation to the downstream boundary, the model is run for 21 full rotor revolutions (38 wave periods). The computational cost for this simulation to run to completion is 13244 CPU hours.

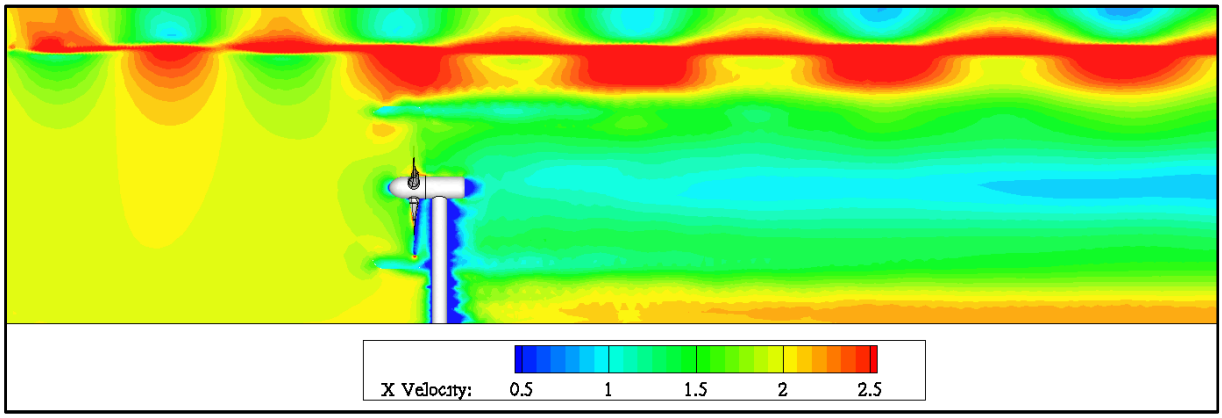

Figure 8: An illustration of the stream-wise component of velocity across a vertical centreline plane.

Figure 8 illustrates the stream-wise component of velocity taken across a vertical centreline cut plane. The wave boundary condition is clearly visible, represented by a characteristic orbital pattern in both the air and water phases. Downstream of the turbine the wave orbitals appear to flatten, suggesting the imposition of a shallow water constraint on the waves by the decelerated core flow generated by the turbine.

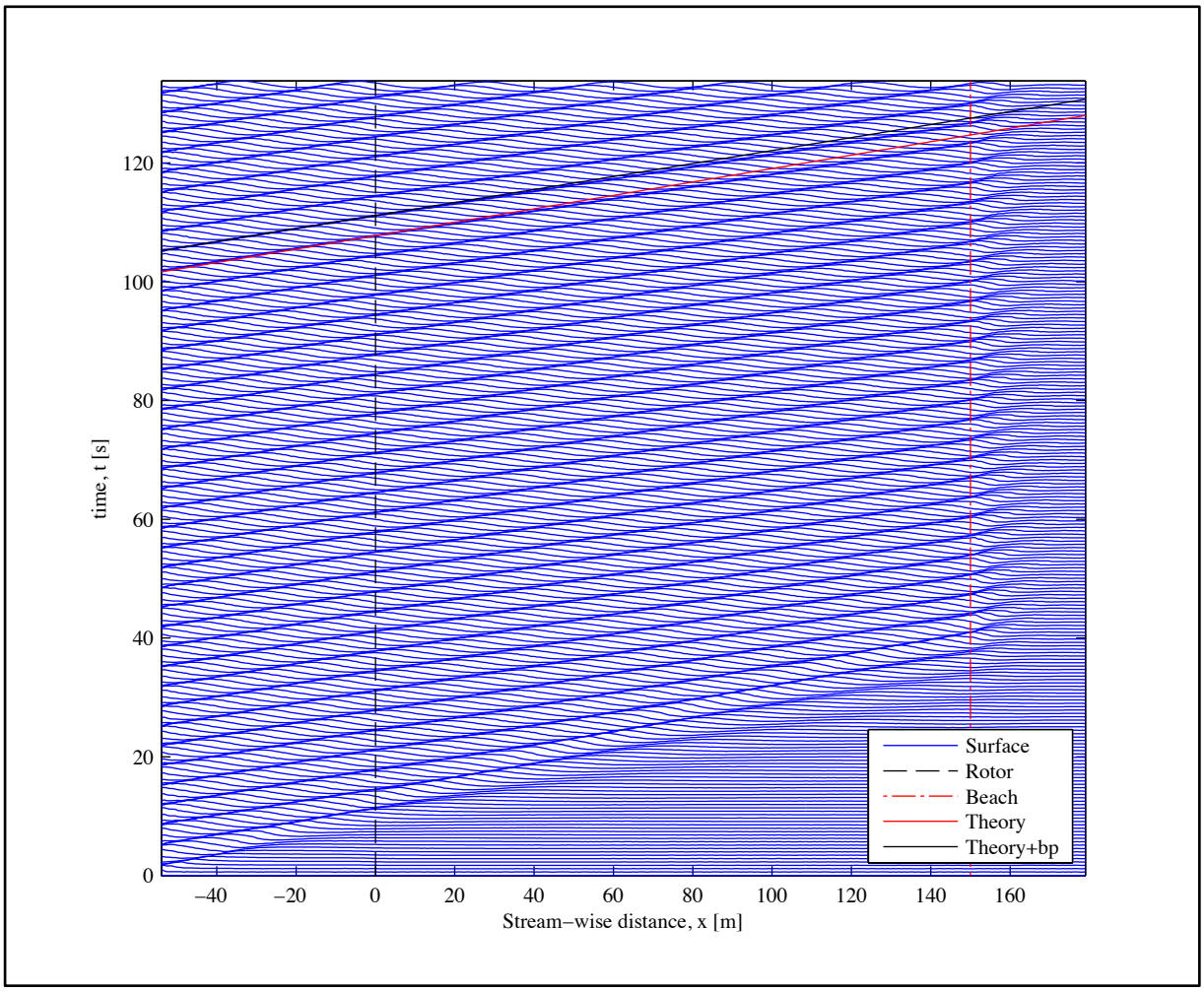

Figure 9: Time evolution of water surface along flume centreline.

Figure 9 illustrates a wave ‘waterfall’ plot for the blade resolved simulation showing the propagation of the wave field through the domain as a function of time. The solid red line labelled ‘Theory’ indicates the predicted progression of a wave crest calculated from intermediate depth first order wave theory. Here, as discussed in section 3, the gradient of this line corresponds to the inverse of wave speed.

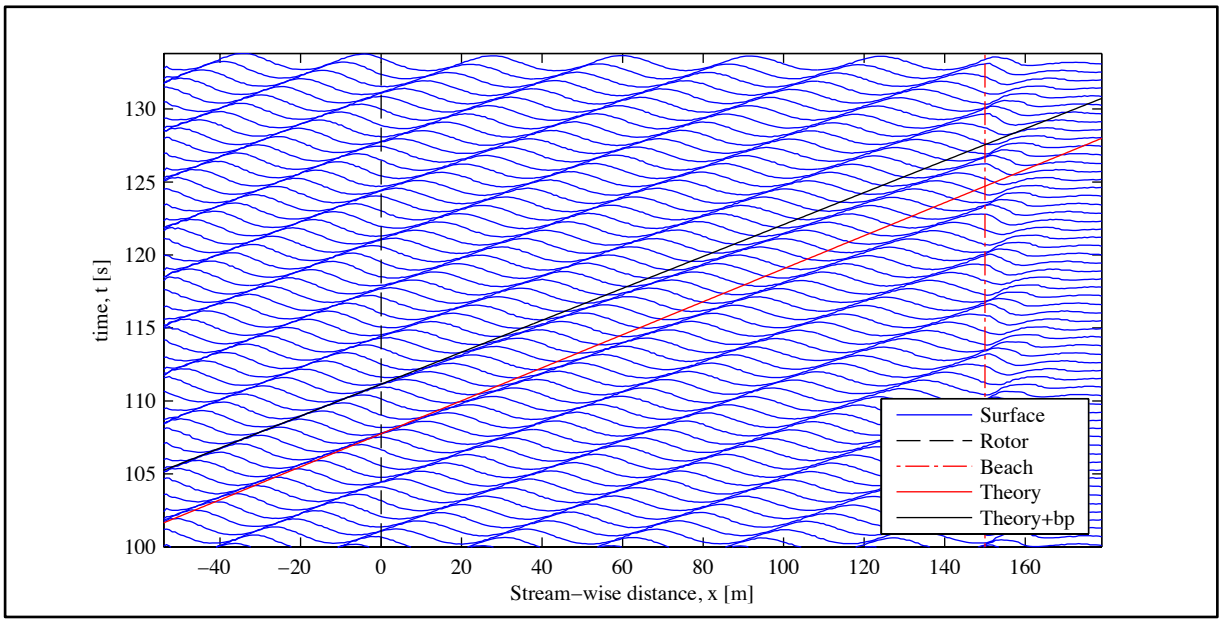

Figure 10: Time evolution of water surface along flume centreline – detailed view of Figure 9.

A clear acceleration (change of gradient) is visible as the waves pass over the turbine (Figure 9, Figure 10), with waves arriving at the numerical beach approximately 1.3 seconds before that predicted first order theory. Some of this disparity is accounted for by the increase in current velocity of the bypass flow (solid black line labelled 'Theroy+bp'). However a difference of around 0.7 seconds remains. It is suggested here that a blocking effect of the core flow on the wave field could be responsible, causing the waves to adopt a shallow water character (higher wave speed and flattened orbitals) when passing over the wake of the turbine.

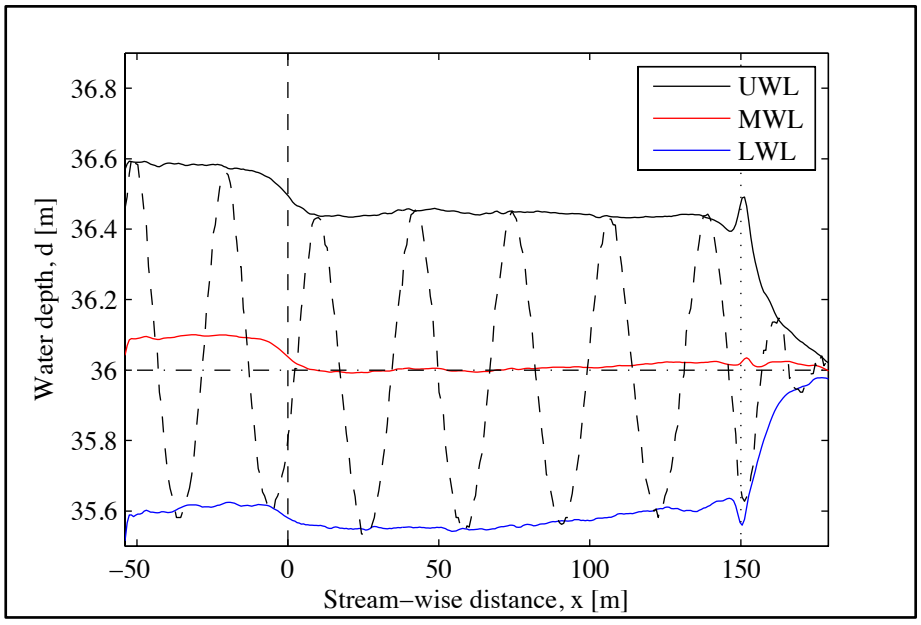

Figure 11: Upper, lower and mean water levels along flume centreline.

Figure 11 details the upper, mid and lower water levels (UWL, MWL and LWM) for the quasi-steady wave field shown in Figure 10. Full upper and lower water level traces are extracted for each wave period *T,* collected and then averaged to produce the bounds (UWL and LWL) illustrated in Figure 11. The MWL is taken as the average of the upper and lower levels. A clear drop in MWL is visible in Figure 11 indicating an extraction of hydrostatic head by the turbine. Also evident in Figure 11 is the influence of the beach damping zone on the wave field. Upon entering the damped zone a brief increase in wave height is shown, followed by a sharp decrease to negligible values at the channel's outlet.

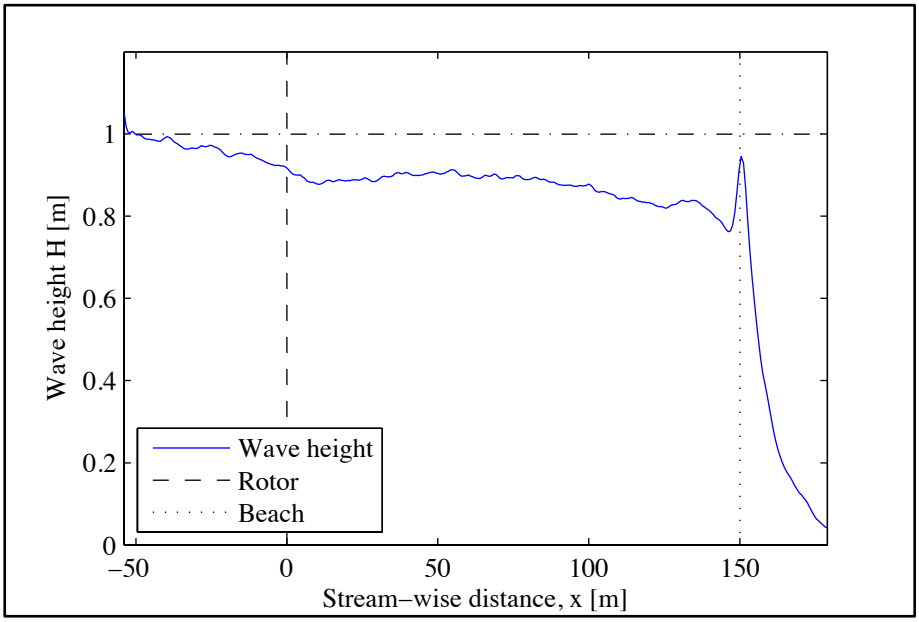

Figure 12: Wave height along flume centreline.

This change in significant wave height *H* (UWL – LWL) is shown explicitly in Figure 12. Plotting *H* as a function of stream-wise distance highlights a possible interaction between the turbine and the associated wave field, with a decrease in *H* of approximately 10% occurring across the rotor. This decrease is partly expected from the increase in wave celerity shown in Figure 10, with a reduction in wave height consistent with conservation of power in the wave train. It is of course possible that the turbine is also be capable of extracting additional power from the wave field, a topic that will be further studied in future deliverables (WG3 WP1 D6/7).

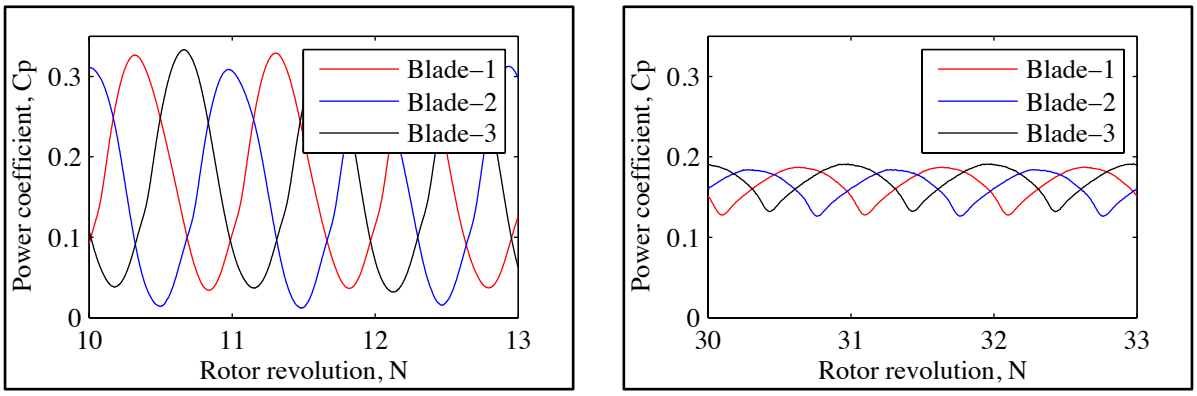

(a) Waves (b) Rigid lid

Figure 13: Unsteady power coeffient for each rotor blade over nine rotor revolutions.

Figure 13 illustrates the component power coefficient traces for a rotor operating beneath a wave field (a) and for the same rotor operating beneath a rigid lid (b). The rigid lid profiles provided here are shown as a point of reference to aid in the assessment of the wave model functionality. Whilst the simulations are similar, direct comparison cannot be made as this rigid lid solution employs a vertically sheared velocity profile whilst the wave model employs a uniform current with waves.

Figure 13 (a) (waves) illustrates large power coefficient fluctuations that are of an approximate sinusoidal nature. The corresponding fluctuations shown in Figure 13 (b) (rigid lid) are of much smaller amplitude and exhibit the features of a squared sinusoid. These plots demonstrate the presence of a large unsteady power component transmitted from the free surface waves to the rotor.

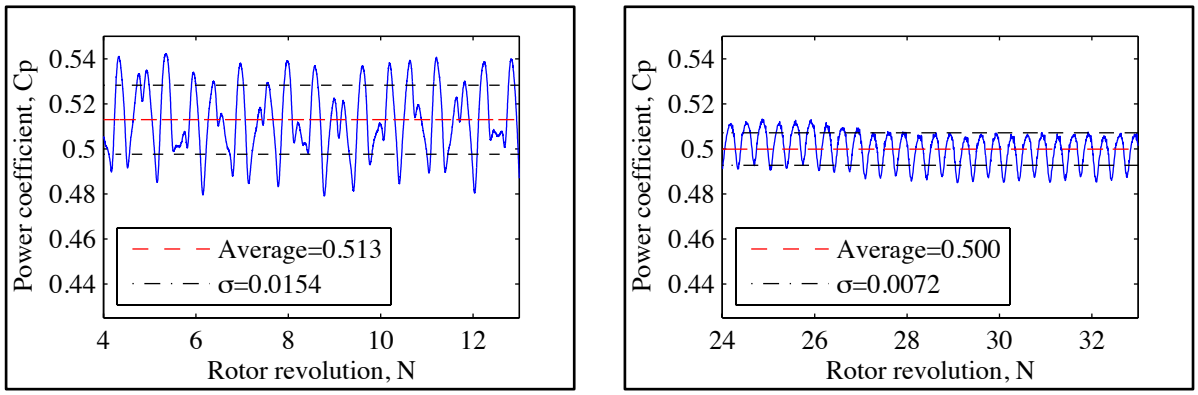

(a) Waves (b) Rigid lid

Figure 14: Overall unsteady power across nine rotor revolutions.

Figure 14 illustrates the overall power fluctuations (per blade component sum). Figure 14 (b) (rigid lid) shows a clear repeating pattern, of an approximate sine squared form, whilst Figure

14 (a) (waves) shows a seemingly random trace with a standard deviation of around twice that of the rigid lid case.

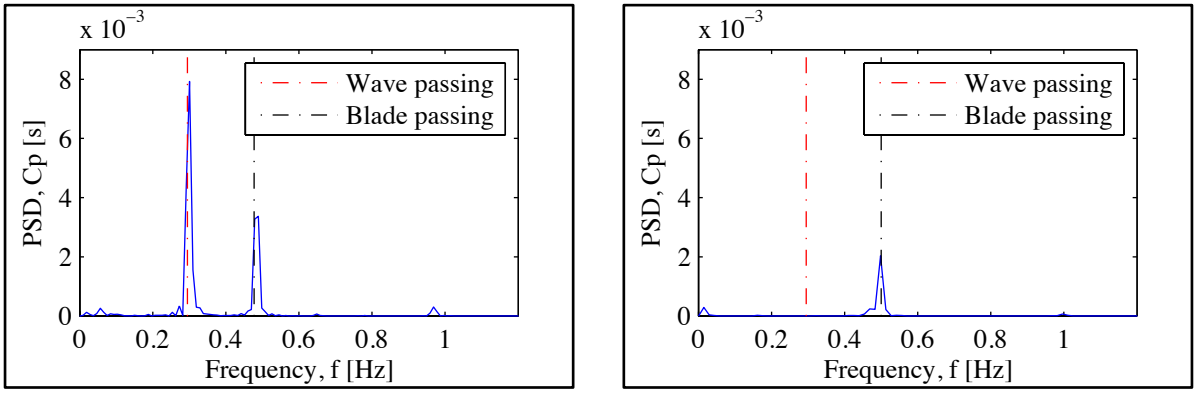

(a) Waves (b) Rigid lid

Figure 15: Power coefficient power spectrum.

The source of these fluctuations is clearly shown in Figure 15, which illustrates the power spectra of the two unsteady C_P traces shown in Figure 14. Figure 15 (b) contains a single peak coincident with the blade passing frequency containing unsteady components from the movement of the blade through the vertically sheared velocity profile and, to a lesser extent, tower passing. Two distinct peaks are shown in Figure 15 (b) at frequencies coincident with both blade passing and wave passing. The power content of the wave passing peak is shown to be around 3 times that of the blade passing peak indicating that, for the present case, the wave field dominates unsteady contributions to turbine power.

Similar trends have been observed for the streamwise components of turbine thrust.

5 Conclusions

The blade resolved tidal turbine model presented in WG4 WP1 D4 has been extended to incorporate a free surface wave capability. Modifications to the previous model include a vertical extension of the numerical grid to include an air phase above the water; modified velocity and phase inlet boundary conditions capable of generating the required wave field, and tuned beach damping zone at the outlet of the domain.

The functionality of these modifications is demonstrated by via an example turbine simulation incorporating free surface waves. This solution is subsequently analysed, demonstrating the capability of the new wave model for application to the study of a range of wave-turbine interaction problems. The results of these future studies will be reported in subsequent deliverables (WG4 WP1 D6/7).

6 Bibliography

ANSYS Inc. (2012). *ANSYS FLUENT 14.5 Theory Guide.* ANSYS Inc.

ANSYS Inc. (2012). *ANSYS FLUENT 14.5 User's Guide.* ANSYS Inc.

Fleming, C. F., McIntosh, S. C., & Willden, R. H. (2012). *WG3 WP1 D4: Performance and Wake Structure of a Full-Scale Horizontal Axis Axial Flow Turbine.* University of Oxford.

Gretton, G. I., & Ingram, D. I. (2011). *WG3 WP5 D1: Development of a computational fluid dynamics model for a horizontal axis tidal current turbine.* University of Edinburgh. PerAWaT Project, Energy Technologies Institute.

McIntosh, S. C., Fleming, C. F., & Willden, R. H. (2010). *WG3 WP1 D1: Report on Model Setup for Horizontal Axis Axial Flow Turbines.* University of Oxford.

McIntosh, S. C., Fleming, C. F., & Willden, R. H. (2011). *WG3 WP1 D3: Performance and wake structure of a model horizontal axis axial flow turbine.* University of Oxford.